# ISO-LWS observations of Herbig Ae/Be stars. I. Fine structure lines

Astron. Astrophys. 346, 604–616 (1999)

ASTRONOMY AND ASTROPHYSICS

# ISO-LWS observations of Herbig Ae/Be stars⋆

## I. Fine structure lines

**D. Lorenzetti[1], E. Tommasi[2], T. Giannini[1,3,4], B. Nisini[4], M. Benedettini[4], S. Pezzuto[4], F. Strafella[5], M. Barlow[6], P.E. Clegg[7], M. Cohen[8], A.M. Di Giorgio[4], R. Liseau[9], S. Molinari[10], F. Palla[11], P. Saraceno[4], H.A. Smith[12], L. Spinoglio[4], and G.J. White[7]**

[1] Osservatorio Astronomico di Roma, via Frascati 33, I-00040 Monte Porzio, Italy
[2] Agenzia Spaziale Italiana, via di Villa Patrizi 13, I-00161 Roma, Italy
[3] Istituto Astronomico, Università La Sapienza, via Lancisi 29, I-00161 Roma, Italy
[4] Istituto di Fisica Spazio Interplanetario – CNR Area Ricerca Tor Vergata, via Fosso del Cavaliere, I-00133 Roma, Italy
[5] Dipartimento di Fisica, Università di Lecce, I-73100 Lecce, Italy
[6] Department of Physics and Astronomy, University College London, Gower Street, London WC1E 6BT, UK
[7] Queen Mary and Westfield College, University of London, Mile End Road, London E1 4NS, UK
[8] Radio Astronomy Laboratory, 601 Campbell Hall, University of California, Berkeley, CA 94720, USA
[9] Stockholm Observatory, S-133 36 Saltsjöbaden, Sweden
[10] IPAC/Caltech, MS 100-22, Pasadena, California, USA
[11] Osservatorio Astrofisico di Arcetri, Largo E.Fermi 5, I-50125 Firenze, Italy
[12] Harvard-Smithsonian Center for Astrophysics, 60 Garden Street, Cambridge, MA 02138, USA

Received 25 November 1998 / Accepted 11 March 1999

**Abstract.** We present the results of the first spectrophotometric survey of a sample of eleven Herbig Ae/Be stars (HAEBE) obtained with the Long Wavelength Spectrometer (LWS) on board the Infrared Space Observatory (ISO). The [OI] 63$\mu$m and the [CII] 158$\mu$m lines are observed in all the investigated sources, while the [OI] 145$\mu$m transition, due to its relative faintness, sometimes remains undetected. By comparing line intensity ratios with model predictions, photodissociation, due to the UV photons from the central star, results the dominating excitation mechanism although contributions of C-shocks to the [OI] emission cannot be ruled out. A clear example for the presence of a photodissociation region (PDR) illuminated by an HAEBE is shown by LWS spectroscopic mapping of NGC 7129. Some diagnostic probes of the radiation field and density are provided for the objects in our sample: these substantially agree with the known characteristics of both the star and its circumstellar environment, although the observed ratio [OI]63/[OI]145 tends to be smaller than predicted by PDR models. The most likely explanation for this behaviour is self-absorption at 63$\mu$m by cold atomic oxygen. Fine structure lines of the ionised species [OIII], [NII] were detected whenever the star had a spectral type of B0 or earlier; in particular, around the star CoD-42°11721, besides a compact HII region, evidence is given for an extended low electron density ionised region. Finally, molecular line emission is associated with stars powering a CO outflow, and clumpy PDR models, better than C-shock models, predict for them relative cooling (CO *vs* OI and CO *vs* OH) similar to the observed ones.

**Key words:** stars: circumstellar matter – stars: pre-main sequence – infrared: ISM: lines and bands – infrared: stars

### 1. Introduction

The environments immediately surrounding Herbig Ae/Be (HAEBE) stars have been widely studied at IR and sub-mm wavelengths. These data have indicated how studying the cool circumstellar (CS) material can probe the inter-relationships between the star formation modalities and properties of the parent cloud. Many observational characteristics can show these interactions: the presence of reflection nebulosity and dust emission in the millimeter continuum; outflow motions detected by CO emission and Herbig-Haro (HH) objects; strong winds and P-Cyg line profiles. An unbiased picture of the close neighbourhood of HAEBE is now provided by ISO-LWS which samples the physical scale where the observed phenomena occur and provides full spectrophotometry in the far IR (43 - 196.7$\mu$m), a range hitherto unexplored by means of spectroscopic airborne observations. The one source whose FIR spectrum has been measured, HD 200775, appears to be described with a clumpy PDR (Chokshi et al. 1988).

The physical conditions of the gas and dust surrounding some HAEBE stars have been studied by Fuente et al. (1990, 1992), who noticed that clouds have larger IR luminosities than those of the stars, indicating the presence of an additional heat-

*Send offprint requests to*: D. Lorenzetti (dloren@coma.mporzio.astro.it)

⋆ Based on observations with ISO, an ESA project with instruments funded by ESA Member States and with the participation of ISAS and NASA

**Table 1.** Parameters of the observed HAEBE.

| Source | Spectral Type | $L_{bol}$ ($L_\odot$) | $A_v$ (mag) | Outflow Activity | distance (pc) | Extendness 50/100$\mu$m | Extendness 1.3mm | Companion | Location |
|---|---|---|---|---|---|---|---|---|---|
| LkH$\alpha$198 | B-Ae | 340 | 4.5 | CO/HH | 600 | Y | Y | IR | L1265 |
| V376 Cas | B5 | 517 | 5.2 | HH | 600 | | Y | opt. | L1265 |
| HD 97048 | B9.5 | 30 | 1.3 | | 150 | | | | Cha I |
| IRAS 12496-7650 | A | 50 | 11 | CO | 250 | | N | | Cha II |
| CoD-42°11721 | B0 | 1120 | 7.1 | | 400 | Y | Y | | Anon. |
| MWC 297 | B1.5 | 923 | 8 | | 250 | Y | Y | neg.result | Aquila Rift |
| R CrA | A5 | 132 | 1.9 | CO/HH | 150 | Y | | IR/mm | NGC 6729 |
| PV Cep | A5 | 100 | 0.4−9.5 | CO/HH | 500 | N | N | | L1158 |
| V645 Cyg | O7 | 1.3 $10^5$ | 4.9 | CO/HH | 6000 | Y | | | Anon. |
| LkH$\alpha$234 | B5/7 | 283 | 3.4 | CO/HH | 1000 | Y | Y | IR | NGC 7129 |
| MWC 1080 | B0 | 1 $10^4$ | 5.3 | CO/HH | 1000 | Y | Y | IR speckle | Anon. |

ing source provided by UV radiation on the molecular gas. The first ISO-LWS data on the Chamaleon II dark cloud, which hosts the HAEBE star IRAS 12496-7650, were discussed by Nisini et al. (1996). The ISO Short Wavelength Spectrometer (SWS) has also contributed to the HAEBE far IR spectroscopy: a full scan (3 - 45$\mu$m) of the source He 3-672 (HD 100546) has been reported by Waelkens et al. (1996) and Malfait et al. (1998); SWS rotational $H_2$ lines of BD+40°4124 have been investigated by Wesselius et al. (1996). The only systematic HAEBE survey of far IR spectra at low resolution, and at shorter wavelengths (8 - 22$\mu$m), has been obtained by the IRAS-LRS. It included 17 objects: LkH$\alpha$198, Elias 1, AB Aur, Haro 13a, VY Mon, LkH$\alpha$25, HD 259431, R Mon, ZCMa, HD 97048, HR 5999, HD 150193, HD 163296, V645 Cyg, MWC1080 (IRAS Science Team 1986); MWC297 and possibly RCrA (Volk & Cohen 1989). Because of its spectrophotometric nature and limited wavelength range, this survey has allowed an accurate investigation of both the continuum shape and the broadest features (e.g. silicate bands), but it could not constrain the excitation mechanisms in the CS cold gas around PMS objects. The only prior systematic survey aimed to clarify this topic, is the pioneering work of Cohen et al. (1988), who investigated the [OI] 63$\mu$m line, at high spectral resolution (R = 4700), from a sample of HH objects and their exciting stars. Their sample is largely dominated by T Tauri stars (which represent the low mass counterparts of HAEBE), and includes one HAEBE, namely R Mon, which remained undetected in that fine structure line. They proposed that a simple combination of J and C shocks could explain the observed line intensities, and suggested that the excess line flux (observed from T Tau) could be due to photodissociation. The indication of shocks is compatible with the collimating role of CS disks, whose presence is widely documented in the case of T Tauri stars. Unfortunately a straightforward scaling of the same disk models to fit the HAEBE SED's has provided inconclusive results. However, spherical reprocessing envelopes appear better able to describe the global SED's of the large majority of HAEBE (Berrilli et al. 1992, Pezzuto et al. 1997). Within this framework, the ISO-LWS observations of HAEBE could provide a tool to discriminate whether the excitation in the FIR is dominated by shocks (as in T Tauri stars), or by photodissociation.

This paper belongs to a series of complementary papers all dealing with ISO observations of HAEBE stars: the others deal with the molecular emission in form of high-J CO and OH rotational transitions (Giannini et al. 1999 Paper II), the study of the FIR continuum (Tommasi et al. 1999 Paper III), and the HI recombination line emission (Benedettini et al. 1998).

## 2. Definition of the sample

Our targets are listed in Table 1: they constitute a small sample (11 objects), which explores a wide range of parameters such as the spectral type (from O7 to A5), the bolometric luminosity (from 30 to 1.3 $10^5$ $L_\odot$), the circumstellar extinction (from a few to more than 10 mag of visual extinction), and the associated outflow activity. Extended emission is reported from the mapping at both 50/100$\mu$m (Natta et al. 1993; Di Francesco et al. 1994, 1998) and 1.3mm (Henning et al. 1998; Fuente et al. 1998). The labels Y, N indicate whether or not the source has been resolved, being the angular resolution of $\sim$ 20, 30 arcsec at 50 and 100$\mu$m respectively and 10-20 arcsec at 1.3mm. Typical sizes range from 30-40 arcsec (far IR) to arcmin scale (1.3mm). In the same table an indication is given for the location of the star and whether or not a close companion has been identified in a specific spectral band.

## 3. Observations and data reduction

The observations were carried out with the Long Wavelength Spectrometer (LWS: Clegg et al. 1996, Swinyard et al. 1996) on board the Infrared Space Observatory (ISO: Kessler et al. 1996) in full grating scan mode (LWS01 AOT). This configuration provides coverage of the 43 - 196.7 $\mu$m range at a resolution R $\sim$ 200, with an instrumental beam size of $\sim$ 80 arcsec. The spectra were oversampled by a factor of 4 and were processed with the off-line pipeline version 6 (OLP V6). The flux calibration is based on observations of Uranus, resulting in an estimated accuracy of about 30% (Swinyard et al. 1996); the wavelength calibration accuracy is a small fraction ($\approx$25%) of the resolu-

**Table 2.** Journal of Observations

| Target | $\alpha$(1950.0) | | | $\delta$ (1950.0) | | | raster parameters | | | $t_{int}$ | $n_{scan}$ | date | orbit |
|---|---|---|---|---|---|---|---|---|---|---|---|---|---|
| | $h$ | $m$ | $s$ | $^\circ$ | $'$ | $''$ | points | step ($''$) | P.A. ($^\circ$) | (sec) | | | |
| LkH$\alpha$198 | 0 | 08 | 47.4 | 58 | 32 | 48 | 1 | – | – | 979 | 5 | 24 Aug 96 | 282 |
| LkH$\alpha$198 off | 0 | 08 | 47.4 | 58 | 32 | 48 | 2×1 | 180/0 | 140 | 1686 | 5 | 24 Aug 96 | 282 |
| V376 Cas | 0 | 08 | 48.1 | 58 | 33 | 23 | 1 | – | – | 979 | 5 | 24 Aug 96 | 282 |
| HD 97048 | 11 | 06 | 39.6 | −77 | 23 | 01 | 1 | – | – | 1547 | 9 | 3 Aug 96 | 261 |
| HD 97048 off | 11 | 06 | 39.6 | −77 | 22 | 11 | 2×1 | 180/0 | 90 | 1686 | 5 | 3 Aug 96 | 261 |
| IRAS 12496-7650 | 12 | 49 | 38.0 | −76 | 50 | 45 | 1 | – | – | 3435 | 19 | 11 Mar 96 | 115 |
| IRAS 12496-7650 off | 12 | 49 | 45.4 | −76 | 50 | 33 | 3×3 | 100/100 | 90 | 2735 | 3 | 11 Mar 96 | 115 |
| CoD-42°11721 | 16 | 55 | 33.8 | −42 | 37 | 37 | 3×1 | 100/0 | 90 | 1089 | 4 | 9 Feb 96 | 84 |
| MWC 297 | 18 | 25 | 01.3 | −03 | 51 | 47 | 3×1 | 100/0 | 90 | 5625 | 9 | 23 Oct 97 | 708 |
| R CrA | 18 | 58 | 31.3 | −37 | 01 | 29 | 1 | – | – | 1263 | 6 | 15 Oct 96 | 334 |
| R CrA off | 18 | 58 | 44.6 | −37 | 01 | 49 | 1 | – | – | 2856 | 15 | 15 Oct 96 | 334 |
| PV Cep | 20 | 45 | 23.6 | 67 | 46 | 36 | 1 | – | – | 2781 | 13 | 28 Jul 96 | 255 |
| PV Cep off | 20 | 45 | 23.6 | 67 | 46 | 36 | 2×1 | 180/0 | 155 | 2538 | 7 | 28 Jul 96 | 255 |
| V645 Cyg | 21 | 38 | 10.6 | 50 | 00 | 43 | 3×1 | 100/0 | 81 | 2385 | 5 | 5 Aug 96 | 263 |
| LkH$\alpha$234 | 21 | 41 | 57.6 | 65 | 53 | 07 | 1 | – | – | 2559 | 16 | 17 Feb 97 | 457 |
| LkH$\alpha$234 off | 21 | 41 | 56.7 | 65 | 51 | 30 | 2×6 | 100/100 | 90 | 7415 | 4 | 17 Nov 96 | 367 |
| MWC 1080 | 23 | 15 | 14.6 | 60 | 34 | 19 | 1 | – | – | 1405 | 8 | 25 Aug 96 | 283 |
| MWC 1080 off | 23 | 15 | 14.6 | 60 | 34 | 00 | 2×2 | 100/100 | 90 | 3088 | 5 | 25 Aug 96 | 283 |

tion element, i.e. 0.07 $\mu$m in the range 43-90 $\mu$m and 0.15 $\mu$m in the range 90-196.7 $\mu$m. A spectrum is composed by ten subspectra, each from one of the ten detectors, thus the steps of the data reduction are: averaging the different spectral scans after removing the glitches due to the impact of cosmic rays; correcting the low-frequency fringes which result from interference along the optical axis with off axis emission (Swinyard et al. 1996).

An evaluation of possible contamination from a large scale emission component is obtained by taking additional spectra adjacent to the source. In most cases these OFF source measurements were obtained by means of raster maps oriented to sample the outflow gas. Since the total integration time spent at the OFF positions is comparable to that ON source, the individual map points can be co-added to effectively remove any contribution not related to the central source or separately used to investigate possible local features. Table 2 reports the Journal of observations. For each entry ON or OFF source positions are indicated: in Columns 2 to 7, the coordinates of the pointed position (in the case of a raster map they indicate the map center); the parameters of the raster, namely the individual positions (m×n - Column 8), where m is along the direction of position angle (P.A. given in Column 10) and n perpendicularly, in Column 9 the spacing between the raster position (step) is given for both directions; the total integration time (Column 11) obtained by means of a number of subsequent scans (Column 12); finally the date and orbit numbers are given in Columns 13 and 14 respectively.

## 4. Results

The FIR spectra towards HAEBE stars consist of emission lines superimposed on a continuum. In Figs. 1, 2 and 3 selected portions of the continuum subtracted LWS spectra are reported for all the observed sources. Discussion of both the continuum shape and a quantitative comparison with IRAS-PSC data, is reported in a separate paper by Tommasi et al. (1999 - Paper III).

The line analysis was performed on the defringed single detector spectra after subtracting a polynomial function which fitted the continuum and then using a single (or double in case of blending) gaussian function. The errors on the line intensities correspond to a 1$\sigma$ statistical uncertainties derived from the *rms* fluctuations adjacent to the line. The criteria adopted for line detection are the following: *i)* signal to noise ratio S/N $\geq$ 3; *ii)* distance between observed and rest wavelength comparable to the wavelength calibration accuracy, namely a small fraction ($\approx$ 25%) of the resolution element ($\approx$ 0.07 and 0.15 $\mu$m for short and long wavelength detectors respectively); *iii)* line width compatible with the nominal value of the relative detector ($\approx$ 0.30 and 0.60 $\mu$m). The fluxes of the detected lines are given in Table 3. We note that, given their closeness, the sources LkH$\alpha$198 and V376 Cas are only marginally disentangled by the LWS beam. Moreover for LkH$\alpha$198, LkH$\alpha$234 and RCrA significant contributions to the FIR emission could come from their mid-infrared and mm-wavelength companions: LkH$\alpha$198IR and LkH$\alpha$198MM (Sandell & Weintraub 1994; Lagage et al. 1993) in the first field; IRS6 (Weintraub et al.1994; Cabrit et al. 1997) in the second field; and IRS7 (Henning et al. 1994) in the third.

The OFF source line intensities are given in Table 4 and correspond to an average of all *off*-positions (see Table 2) whenever the same spectral features occur at comparable intensities (within the errors); otherwise, all the raster map contributions are individually reported. This is the case of the maps around LkH$\alpha$234 and MWC 1080, which are separately discussed in

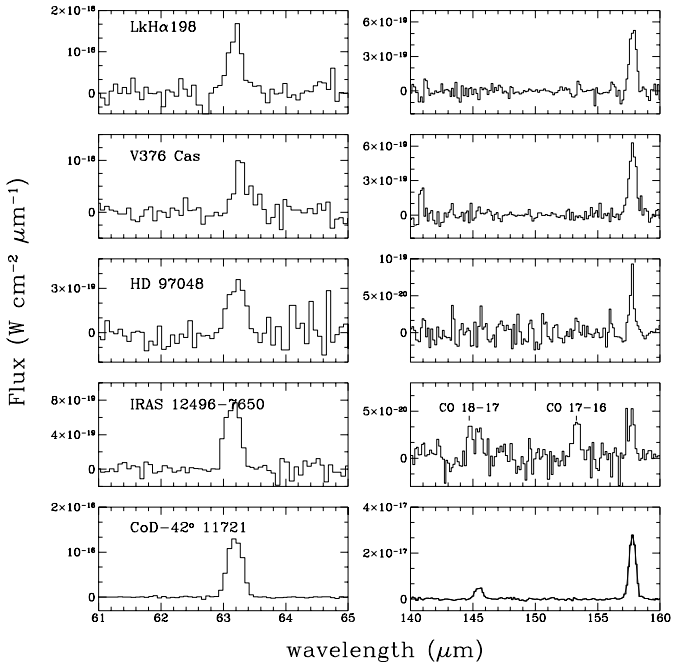


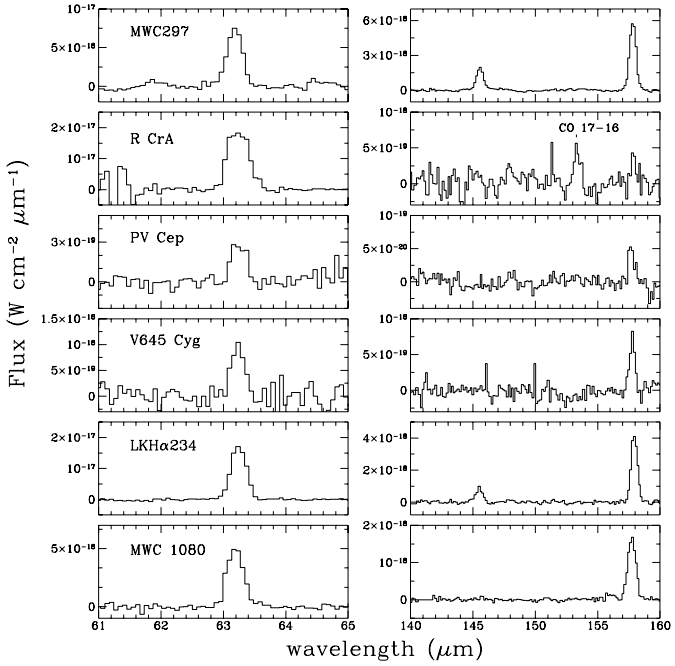


**Fig. 1.** Continuum subtracted LWS spectra of the observed HAEBE stars: selected ranges containing the [OI] (63 and 145$\mu$m) and [CII] (158$\mu$m) lines. Other detected lines are labelled in the relative panel

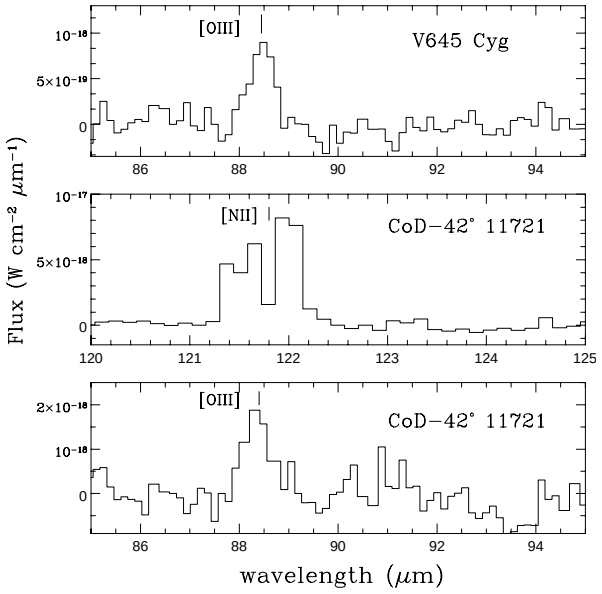


**Fig. 2.** Same as Fig. 1: selected ranges containing the [OIII] (88.3$\mu$m) and [NII] (121.8$\mu$m) lines.

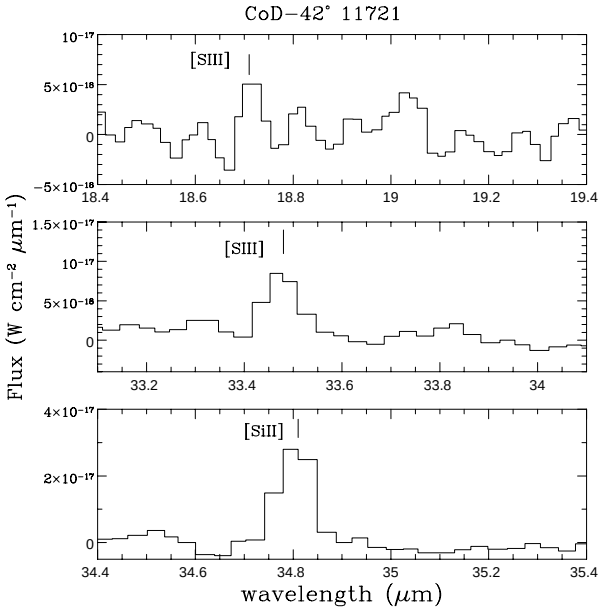


**Fig. 3.** Continuum subtracted SWS spectra of CoD-42°11721: selected ranges containing the [SIII] (18.7, 33.5$\mu$m) and [SiII] (34.8$\mu$m) lines.

Sects. 5.2 and 5.3. The first map (covering $\approx 3\times10$ arcmin) includes the NGC 7129 region, which exhibits several signposts of active star formation: two HAEBE stars LkH$\alpha$234 and BD+65°1637, the former associated with an embedded companion (Weintraub et al. 1994); a FIR source (Bechis et al. 1978); a complex structure of molecular outflows (Mitchell & Matthews 1994); several HH objects and jets (Ray et al. 1990); and water masers (Sandell & Olofsson 1981). Most of these objects are included within the LWS spectrophotometric raster scan. The second map (covering $\approx 3\times3$ arcmin) is intended to investigate the extended CO outflow from MWC 1080 (Cantó et al. 1984).

From Tables 3 and 4 it can be seen that the [OI] (63, 145$\mu$m) and the [CII] (158$\mu$m) lines are commonly observed in both the *on* and *off* source spectrum. Because of the higher excitation temperature, the OI lines are brighter *on* source, while the CII line tends to have comparable intensities (within a factor of 2) at all the positions. Higher ionization lines ([OIII] and [NII]) are detected toward sources with spectral type earlier than B0

**Table 3.** ON-Source line intensities

| Source | $\lambda_{obs}$ ($\mu$m) | Identification | Flux ($10^{-19}$ W cm$^{-2}$) | Notes |
|---|---|---|---|---|
| **LkH$\alpha$198** | 63.20 | [OI] | $4.1 \pm 0.5$ | |
| | 157.75 | [CII] | $5.6 \pm 0.4$ | |
| | 162.72 | CO (J=16-15) | $1.4 \pm 0.4$ | |
| **V376 Cas** | 63.22 | [OI] | $2.2 \pm 0.7$ | |
| | 157.82 | [CII] | $5.4 \pm 0.4$ | |
| **HD 97048** | 63.19 | [OI] | $1.9 \pm 0.3$ | |
| | 157.82 | [CII] | $0.7 \pm 0.1$ | |
| **IRAS 12496-7650** | 63.15 | [OI] | $4.3 \pm 0.3$ | |
| | 130.42 | CO (J=20-19) | $0.14 \pm 0.05$ | |
| | 137.13 | CO (J=19-18) | $0.27 \pm 0.05$ | |
| | 144.71 | CO (J=18-17) | $0.42 \pm 0.05$ | d |
| | 145.49 | [OI] | $0.31 \pm 0.08$ | d |
| | 153.32 | CO (J=17-16) | $0.54 \pm 0.06$ | |
| | 157.65 | [CII] | $0.4 \pm 0.1$ | |
| | 162.84 | CO (J=16-15) | $0.46 \pm 0.04$ | |
| | 173.62 | CO (J=15-14) | $0.36 \pm 0.05$ | |
| **CoD-42°11721** | 18.71 | [SIII] | $2.6 \pm 0.8$ | |
| SWS | 33.45 | [SIII] | $6.8 \pm 0.7$ | |
| | 34.80 | [SiII] | $27 \pm 2$ | |
| | 63.17 | [OI] | $400 \pm 6$ | |
| LWS | 88.39 | [OIII] | $15 \pm 3$ | |
| | 121.83 | [NII] | $36 \pm 8$ | |
| | 145.45 | [OI] | $37 \pm 3$ | |
| | 157.77 | [CII] | $205 \pm 3$ | |
| **MWC 297** | 63.17 | [OI] | $24 \pm 1$ | |
| | 145.53 | [OI] | $12.0 \pm 0.5$ | |
| | 157.80 | [CII] | $41.6 \pm 0.5$ | |
| **R CrA** | 63.18 | [OI] | $58 \pm 1$ | |
| | 65.21 | OH | $5 \pm 1$ | d |
| | 65.76 | CO (J=40-39) | $4 \pm 1$ | d |
| | 66.98 | em. feat. | $4 \pm 1$ | |
| | 79.08 | OH | $4 \pm 1$ | |
| | 84.60 | OH | $9 \pm 2$ | |
| | 124.12 | CO (J=21-20) | $5 \pm 1$ | |
| | 137.06 | CO (J=19-18) | $4 \pm 1$ | d |
| | 153.46 | CO (J=17-16) | $4.2 \pm 0.8$ | b |
| | 157.81 | [CII] | $3 \pm 1$ | |
| | 162.95 | CO (J=16-15) | $7.2 \pm 0.8$ | a |
| | 173.69 | CO (J=15-14) | $7.8 \pm 0.6$ | a |
| | 185.98 | CO (J=14-13) | $4.6 \pm 0.9$ | |
| **PV Cep** | 63.22 | [OI] | $2.1 \pm 0.3$ | |
| | 157.79 | [CII] | $0.36 \pm 0.07$ | |
| **V645 Cyg** | 63.18 | [OI] | $10 \pm 1$ | |
| | 88.45 | [OIII] | $5.4 \pm 0.9$ | |
| | 157.80 | [CII] | $16 \pm 1$ | |
| **LkH$\alpha$234** | 63.20 | [OI] | $55 \pm 1$ | |
| | 145.44 | [OI] | $6.7 \pm 0.4$ | d |
| | 157.83 | [CII] | $32.3 \pm 0.6$ | |
| | 162.89 | CO (J=16-15) | $3.0 \pm 0.7$ | |
| | 173.56 | CO (J=15-14) | $1.6 \pm 0.5$ | |
| | 185.92 | CO (J=14-13) | $1.3 \pm 0.4$ | |
| **MWC 1080** | 63.20 | [OI] | $14.4 \pm 0.6$ | |
| | 145.52 | [OI] | $1.2 \pm 0.4$ | |
| | 157.82 | [CII] | $13.0 \pm 0.4$ | |

*Notes to the Table:*

a FWHM marginally larger or smaller than the nominal value of the relative detector

b distance between observed and rest wavelength ($\Delta\lambda$) marginally exceeding the resolution element

d deblended

and molecular transitions (CO and OH) are associated with the low luminosity and embedded objects.

## 5. Discussion

### *5.1. [OI] and [CII] lines*

The [OI] 63$\mu$m and [CII] 158$\mu$m fine structure lines are by far the strongest features observed and are, together with [OI] 145$\mu$m, a diagnostic of the excitation mechanism. In order to ascertain the contribution intrinsic to the source, we report the fluxes obtained by subtracting the off-source contribution in Table 5, along with the propagating uncertainties. This procedure does not severely affect the OI line intensities, which are much stronger on-source, but has a definite effect on the CII lines because of its ubiquity at comparable intensities.

Since a comparison between line intensities and model predictions can be constrained with upper limits, we evaluated the data values for those cases with no clear detection. In Table 5 we report the results obtained by computing a 3$\sigma$ value of the *rms*-continuum at 145$\mu$m, whenever no significant [OI] line flux was detected. A comparison between the [OI] 63$\mu$m and the IRAS 60$\mu$m fluxes (Column 5), indicates that the line contribution never affects (by more than 0.2%) the in-band photometric values, the only marginal exception being represented by CoD-42° 11721, whose line to continuum relative contribution is $\sim 0.7\%$

In Fig. 4 the observed line intensity ratios (see Table 5) are superimposed on a grid of photodissociation models (Kaufman et al. 1998). Differences between the line intensity predictions of this model and those of other PDR models (e.g. Hollenbach, Takahashi & Tielens 1991, hereinafter HTT) stem from the inclusion of an additional heating source, namely the ejection of photoelectrons from PAH and small grains. These latter are essential ingredients of the HAEBE environments, as confirmed by several dedicated observations (see e.g. Brooke et al. 1993 and references therein; Prusti et al. 1994). The extra heating source makes a substantial difference since smaller values of both density and radiation field are derived for a given set of line ratios compared to the other PDR models. On the contrary, for a given value of $n$ and $G_o$, the extra heating source increases the column density of warm OI and CII, thus the transition point between CII dominated cooling and OI dominated cooling oc-

**Table 4.** OFF-Source line intensities

| OFF-Source | [OI]63$\mu$m | [OI]145$\mu$m | [CII]158$\mu$m | Other lines |
|---|---|---|---|---|
| | | | Flux ($10^{-19}$ W cm$^{-2}$) | |
| LkH$\alpha$198 | $1.7 \pm 0.6$ | – | $3.4 \pm 0.1$ | |
| HD97048 | – | | $0.3 \pm 0.1$ | |
| IRAS 12496-7650 | – | – | $0.47 \pm 0.09$ | |
| CoD-42° 11721 | $27 \pm 2$ | $2.5 \pm 0.7$ | $87 \pm 2$ | [OIII]88$\mu$m: $6 \pm 2$; [NII]122$\mu$m: $11 \pm 1$ |
| MWC 297 | $3.2 \pm 0.6$ | $3.3 \pm 0.4$ | $15.0 \pm 0.5$ | |
| R CrA | $2.1 \pm 0.3$ | $0.3 \pm 0.1$ | $0.9 \pm 0.1$ | CO(J=16-15): $0.4 \pm 0.1$ |
| PV Cep | – | – | $0.39 \pm 0.06$ | |
| V645 Cyg | – | – | $6.7 \pm 0.2$ | [OIII]88$\mu$m: $8.5 \pm 0.3$ |
| LkH$\alpha$234 1-1 | $3.4 \pm 0.5$ | $< 0.6$ | $4.4 \pm 0.5$ | |
| 1-2 | $19 \pm 1$ | $1.8 \pm 0.5$ | $27.1 \pm 0.6$ | |
| 1-3 | $58 \pm 2$ | $5.0 \pm 0.5$ | $49.7 \pm 0.8$ | |
| 1-4 | $10 \pm 1$ | $1.0 \pm 0.5$ | $12.8 \pm 0.3$ | |
| 1-5 | $3 \pm 1$ | $< 0.6$ | $4.9 \pm 0.4$ | |
| 1-6 | $1.6 \pm 0.9$ | $< 0.3$ | $2.4 \pm 0.2$ | |
| 2-1 | $2.8 \pm 0.7$ | $0.2 \pm 0.1$ | $3.1 \pm 0.2$ | |
| 2-2 | $14 \pm 1$ | $0.7 \pm 0.2$ | $8.2 \pm 0.5$ | |
| 2-3 | $9.7 \pm 0.2$ | $1.4 \pm 0.5$ | $13 \pm 2$ | |
| 2-4 | $3.5 \pm 0.5$ | $0.5 \pm 0.1$ | $6.5 \pm 0.9$ | |
| 2-5 | $2.5 \pm 0.5$ | $< 0.5$ | $3.1 \pm 0.2$ | |
| 2-6 | $1.3 \pm 0.6$ | $< 0.5$ | $2.8 \pm 0.3$ | |
| MWC 1080 1-1 (NW) | $7.1 \pm 0.7$ | – | $8.5 \pm 0.1$ | CO(J=17-16): $0.6 \pm 0.2$ |
| 1-2 (SW) | $4.5 \pm 0.6$ | – | $9.2 \pm 0.2$ | [OIII]88$\mu$m: $1.7 \pm 0.4$ |
| 2-1 (NE) | $6.0 \pm 0.5$ | $0.4 \pm 0.1$ [b] | $8.9 \pm 0.2$ | |
| 2-2 (SE) | $3.0 \pm 0.6$ | – | $7.4 \pm 0.2$ | [OIII]88$\mu$m: $1.4 \pm 0.4$; CO(J=15-14): $0.6 \pm 0.2$ |

*Note to the Table:*

b distance between observed and rest wavelength ($\Delta\lambda$) marginally exceeding the resolution element

curs at lower $n$ and $G_o$. Our ISO-LWS observations indicate that photodissociation can be considered the main excitation source for these lines in HAEBE. J-shock models (e.g. Hollenbach & McKee 1989) can be ruled out, apart the marginal exception represented by IRAS 12496 (see its arrow in Fig. 4 and the discussion in Nisini et al. 1996), since they predict substantially different line ratios: 30 - 200 and 10 - $10^4$ for [OI]63/[OI]145 and [OI]63/[CII]158, respectively. The role of non dissociative C-shocks has to be discussed in more detail since most of the sources are driving molecular outflows. C-shocks models (e.g. Draine et al. 1983) do not predict any substantial [CII] emission, whose excitation is very likely attributable to the exsistence of a PDR, but they are able to give a line intensity ratio [OI]63/[OI]145 which is comparable to the observed values in peculiar gas conditions. The predicted ratio is always greater than 10, but it remains around this value in a narrow range of shock speed (10-20 Km s$^{-1}$ at B$_o$ = 50 $\mu$G and 15-30 Km s$^{-1}$ at B$_o$ = 100 $\mu$G) adopting a pre-shock density n$_H$=$10^4$ cm$^{-3}$, while, increasing the density, the ratio always exceeds the value of 50. Thus, possible contributions of C-shocks to the far IR emission lines cannot be ruled out, but such mechanism can be considered as the main responsible for the gas excitation just in a narrow region of the parameter space.

Although the upper limits and the relatively large errors in the line ratios do not allow an accurate derivation of the PDR parameters (FUV field $G_o$, and density n) for all the sources, nevertheless some useful constraints can be made: the PDR associated with HAEBE seem to have relatively low densities, while the illuminating field is enhanced by a factor $> 10^3$ with

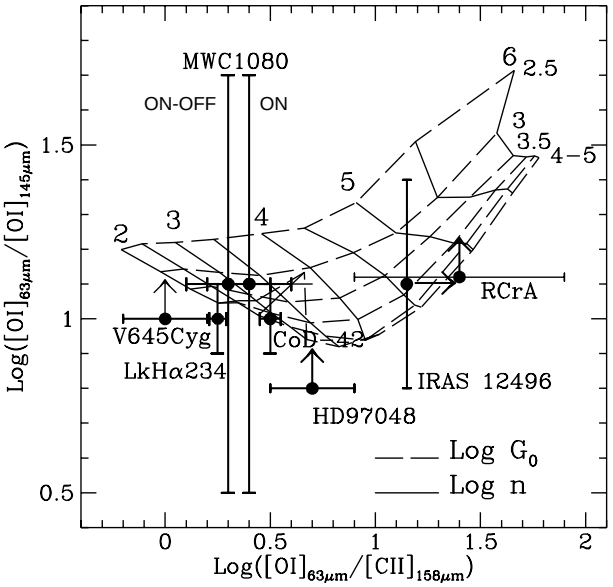


**Fig. 4.** Observed line ratios superimposed to PDR model (see text).

**Table 5.** [OI], [CII] ON-OFF source contributions ($3\sigma$ upper limits) and parameters related to [OI] 63$\mu$m emission

| Source | [OI] 63$\mu$m | [OI] 145$\mu$m | [CII] 158$\mu$m | F[OI] 63$\mu$m | $L_{[OI]63}$ | $\dot{M}$(HI) | $\dot{M}$(CO) | $\dot{M}$([OI]63) |
|---|---|---|---|---|---|---|---|---|
| | Flux ($10^{-19}$ W cm$^{-2}$) | | | IRAS 60$\mu$m | ($L_\odot$) | ($M_\odot$ yr$^{-1}$) | | |
| LkH$\alpha$198 | $2.4 \pm 0.8$ | $< 1.2$ | $2.2 \pm 0.2$ | $6.3\ 10^{-4}$ | $3.3\ 10^{-2}$ | $2.0\ 10^{-7}(1)$ | $3.2\ 10^{-7}(2)$ | $3.3\ 10^{-6}$ |
| V376 Cas | $<1.0$ | $< 0.9$ | $2.0 \pm 0.4$ | – | – | – | – | – |
| HD97048 | $1.9 \pm 0.3$ | $< 0.3$ | $0.4 \pm 0.01$ | $1.0\ 10^{-3}$ | $1.6\ 10^{-3}$ | – | – | $1.6\ 10^{-7}$ |
| IRAS 12496-7650 | $4.3 \pm 0.3$ | $0.31 \pm 0.08$ | $< 0.3$ | $1.5\ 10^{-3}$ | $1.0\ 10^{-2}$ | – | – | $1.0\ 10^{-6}$ |
| CoD-42° 11721 | $373 \pm 6$ | $34 \pm 4$ | $118 \pm 4$ | $7.0\ 10^{-3}$ | 2.3 | $> 5\ 10^{-7}$ (3) | – | $2.3\ 10^{-4}$ |
| MWC 297 | $20 \pm 2$ | $9 \pm 1$ | $26 \pm 1$ | $8.0\ 10^{-4}$ | $4.7\ 10^{-2}$ | $1.2\ 10^{-6}(1)$ | – | $4.7\ 10^{-6}$ |
| R CrA | $56 \pm 1$ | $< 4.3$ | $2 \pm 1$ | $3.3\ 10^{-3}$ | $4.8\ 10^{-2}$ | – | $3.3\ 10^{-7}$ (2) | $4.8\ 10^{-6}$ |
| PV Cep | $2.1 \pm 0.3$ | $< 0.1$ | $< 0.2$ | $1.5\ 10^{-3}$ | $2.0\ 10^{-2}$ | – | $5.9\ 10^{-8}$ (2) | $2.0\ 10^{-6}$ |
| V645 Cyg | $10 \pm 1$ | $< 0.9$ | $9 \pm 1$ | $1.0\ 10^{-3}$ | 13.7 | $4.5\ 10^{-7}$(5) | $1.4\ 10^{-6}$(2) | $1.4\ 10^{-3}$ |
| LkH$\alpha$234 | $53 \pm 1$ | $5.2 \pm 0.4$ | $29.5 \pm 0.7$ | $3.3\ 10^{-3}$ | 2.0 | $1.4\ 10^{-7}$ (1) | $4.0\ 10^{-6}$ (4) | $2.0\ 10^{-4}$ |
| MWC 1080 | $9.3 \pm 0.8$ | $0.8 \pm 0.4$ | $4.5 \pm 0.4$ | $2.3\ 10^{-3}$ | 2.2 | $3.1\ 10^{-6}$ (1) | $3.1\ 10^{-6}$ (2) | $2.2\ 10^{-4}$ |

*References to the Table:*
1. Nisini et al. 1995; 2. Levreault 1988; 3. McGregor & Hyland 1988; 4. Edwards & Snell 1983; 5. Calculated from the Br$\gamma$ flux given by Harvey & Lada 1980.

respect to the interstellar field $G_o$ expressed in units of the average interstellar flux ($1.6\ 10^{-3}$ ergs cm$^{-2}$ s$^{-1}$, Habing 1968). This latter circumstance suggests a stellar rather than an interstellar origin for the FUV photons. This hypothesis is supported also by the clear correlation between the [CII] 158$\mu$m luminosity *vs.* the bolometric luminosity of the central source shown in Fig. 5. The same is true for the [OI] 63$\mu$m, however, in this latter case, the correlation has to be considered as a necessary but not exclusive condition, because the same relationship also holds in the case of [OI] shock excitation. In a shocked environment in fact, [OI] emission is strictly related to the mass loss rate ($\dot{M}$) which has been demonstrated to correlate with $L_{bol}$ (Levreault 1988).

The two facts that FIR line emission is peaked *on* source and that it likely arises from photodissociation, indicate that PDR's size are reasonably smaller than the LWS beam, which roughly corresponds to 0.04 and 0.4 pc at distances of 100 and 1000 pc respectively. For stellar temperatures between $10^4$ and $3\ 10^4$, the typical size of the associated PDR ranges between 0.01 and 0.06 pc, as derived by Diaz-Miller et al. (1998) who have calculated the structure of the photoionisated and photodissociated regions around Main Sequence stars, taking account for the dust opacity. Although slightly larger values for stellar radii and luminosities are expected for Pre Main Sequence objects, the predicted sizes are well within the LWS beam at any distance, and, as such, are fully in agreement with our results.

The case of CoD-42° 11721 provides reasonable constraints to the values of $G_o$ ($3\ 10^3$ - $10^4 G_o$) and n ($3\ 10^2$ - $10^3$ cm$^{-3}$), because of the good S/N ratios. For this source we have also obtained the SWS spectrum covering the range 2.5-45$\mu$m at a resolution of about 250 (AOT01): we have discussed all the details about SWS observations and data reduction in Benedettini et al. (1998). Emission lines of [SIII] and [SiII] have been clearly detected in the 18-35 $\mu$m range (Fig. 3); the observed intensities are reported in Table 3. [SiII] line emission is expected to be an important tracer of PDR, thus allowing a comparison

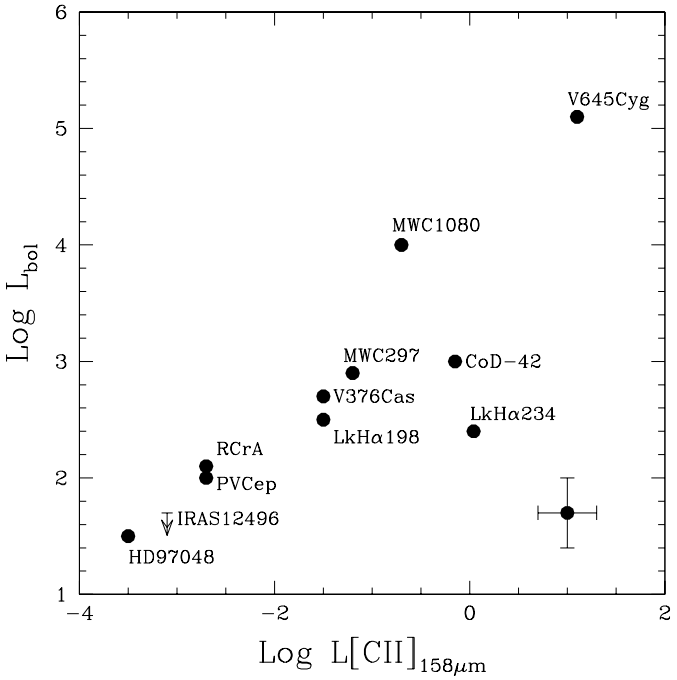


**Fig. 5.** [CII] luminosity *vs.* bolometric luminosity of the central stars. The mean error is indicated by the cross in the bottom right corner.

to be made with models. We evaluate the line ratios of this fine structure line with [OI] and [CII]. The beam at 35$\mu$m ($1.6\ 10^{-8}$ sr) is smaller than that at 63$\mu$m ($1.3\ 10^{-7}$ sr). Accounting for this difference and assuming a unity beam filling factor at both wavelengths, yields a [OI]/[SiII] intensity ratio of $\sim 2$, while the ratio of [CII]/[SiII] remains $<1$. Both these ratios contrast with values $\sim 10^2$ predicted by models (HHT) over a wide range of values for the density and radiation field. However such discrepancy, maybe due to an underabundance of gas-phase Si assumed by models, is confirmed by all other observations available in literature and was pointed out by HTT themselves, who signal

(in their Fig. 17) how [SiII] observations systematically exceed model predictions.

A better agreement is found with models of "clumpy" PDR's (Burton et al. 1990) which predict [OI]/[SiII] and [CII]/[SiII] ratios as low as 12-15 and 1-10 respectively, for densities ranging between $10^4$ and $10^5$ cm$^{-3}$. The comparison of the observed [OI]/[SiII] ratio with models could be uncertain if the 63$\mu$m line is self-absorbed (see below), but the [CII]/[SiII] ratio is in good agreement, which becomes even better allowing for more relaxed beam filling corrections.

From inspection of Fig. 4 we notice that the majority of sources cluster in the density range $10^2$ - 3 $10^3$ cm$^{-3}$, while evidence for relatively high density environments is found for IRAS12496 and R CrA. This picture appears fully compatible with independent observational evidence: ($i$) densities $\sim$ 1-5 $10^3$ cm$^{-3}$ derived for HAEBE by Fuente et al. (1992) through $^{12}$CO and $^{13}$CO mapping; ($ii$) densities $\sim$ 100-200 cm$^{-3}$ derived by Federman et al.(1997) for the PDR associated to the Herbig star HD200775; ($iii$) the CO molecular emission of high J rotational transitions (for a detailed discussion see Sect. 5.5 and Giannini et al. (1999) - hereinafter Paper II) have been detected towards R CrA and IRAS 12496, which both exhibit high density PDR regions indicating an increased column density. Our fit to the CO line intensities allow the derivation of densities $\sim$ $10^5$ - $10^6$ cm$^{-3}$, largely compatible with the PDR diagnostic results.

In Fig. 4 some objects are located in (*x*,*y*) positions characterised by values of the [OI] 63/145$\mu$m ratio which are significantly lower than the model predictions. The most extreme cases are the sources LkH$\alpha$198 and MWC 297 not even reported in the plot and corresponding to (0.0,>0.3) and (0.3,-0.1) respectively. This circumstance suggests the possibility that the [OI] 63$\mu$m line could be self-absorbed by cold ($\lesssim$ 100 K) OI present along the line of sight to the emitting source. Around this temperature and for density values up to $10^7$ cm$^{-3}$, 95% of oxygen atoms are in the ground state; assuming a thermal broadening, a column density of $N_H \sim 10^{22}$ cm$^{-2}$ ($A_V \approx 5$) will result in a reduction of the intensity to 1/3 of its intrinsic value. This occurrence would be enough to relocate LkH$\alpha$198 in the plot to a position which is easier to model (0.5,>0.8) and then provides arguments to cautiously interpret the location of some data points in Fig. 4. If the same absorption were applied to LkH$\alpha$234 the line ratios would diagnose log $G_o \approx 2$ and $\log n \approx 5$: these latter values agree with the conclusions derived below (in Sect. 5.5) and in Paper II. The sources that most likely can exhibit OI absorption are obviously those located within density peaks: out of a sample of 13 HAEBE, Fuente et al. (1998) identified such peaks for the sources LkH$\alpha$198, PV Cep, LkH$\alpha$234 and MWC1080. The case of [OI] 63$\mu$m absorption has been discussed by Saraceno et al. (1998), and several star forming regions have been found so far where this line is detected in absorption (see Kraemer & Jackson 1998, Baluteau et al. 1997). These results suggest the need to refine PDR models including a more realistic morphology of the emitting region (see Liseau et al. 1998) Alternatively, the low values of the [OI] 63/145 observational ratios could be explained by an excess of [OI] 145$\mu$m emission, but, at this time, we are not able to suggest any meaningful motivation for that.

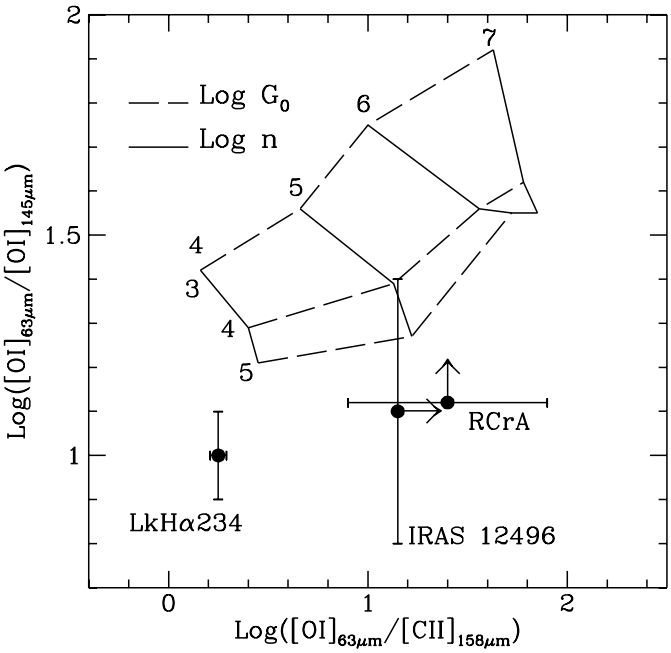


**Fig. 6.** Observed line ratios of sources which exhibit molecular emission superimposed to clumpy PDR models (Burton et al. 1990).

As indicated below (Sect. 5.5), and thoroughly discussed in Paper II, molecular line emission detected by ISO-LWS in three HAEBE is compatible with clumpy PDR models (Burton et al. 1990), where molecular self shielding can move the $C^+$/CO interface closer to the radiation source. To check whether or not this hypothesis is consistent with the fine structure intensity ratios as well, in Fig. 6 we plot the observed data of the three HAEBE associated with molecular emission superimposed to the clumpy PDR model predictions. We notice a marginal agreement that would be reinforced if correction was made for assumed OI absorption.

One other argument in favour of a PDR origin for the fine structure line emission is given by comparing the mass loss rates derived from published values of the HI recombination and CO lines (Columns 7 and 8 of Table 5) and those obtained from the [OI] 63$\mu$m line using the relationship given by Hollenbach (1985) (Column 9 of Table 5). Since the values of $\dot{M}$[OI] systematically exceed (by more than one order of magnitude) the other estimates, we can conclude that an additional component of [OI] emission must be the dominant one, such as the PDR emission.

### *5.2. NGC 7129 line mapping*

Because of its complex morphology, we have mapped a region of size $\approx 3\times10$ arcmin of NGC 7129 with the LWS (see Table 2) detecting the lines of [OI] at 63, 145$\mu$m and [CII] at 158$\mu$m in every map position. In Table 6 the line intensities for each pointing are listed (in Columns 2 to 4), while the isophotal contours of [OI] 63$\mu$m and [CII] 158$\mu$m are shown in Fig. 7. In the same

**Table 6.** [OI], [CII] line intensities in NGC 7129 and derived parameters

| Position | [OI] 63$\mu$m | [OI] 145$\mu$m | [CII] 158$\mu$m | log $G_o$ | | log density |
|---|---|---|---|---|---|---|
| | Flux ($10^{-19}$ W cm$^{-2}$) | | | model | BD+65° | (cm$^{-3}$) |
| 1-1 | $3.4 \pm 0.8$ | $< 0.6$ | $4.4 \pm 0.5$ | $1.6 \pm 0.1$ | 1.4 | $3.3 \pm 0.2$ |
| 1-2 | $19 \pm 1$ | $1.8 \pm 0.5$ | $27.1 \pm 0.6$ | $2.37 \pm 0.02$ | 2.1 | $2.6 \pm 0.2$ |
| 1-3 | $58 \pm 2$ | $5.0 \pm 0.5$ | $49.7 \pm 0.8$ | $2.63 \pm 0.02$ | 2.3 | $2.9 \pm 0.2$ |
| 1-4 | $10 \pm 1$ | $1.0 \pm 0.5$ | $12.8 \pm 0.3$ | $2.05 \pm 0.02$ | 1.6 | $3.4 \pm 0.2$ |
| 1-5 | $3 \pm 1$ | $< 0.6$ | $4.9 \pm 0.4$ | $1.62 \pm 0.08$ | 1.2 | $3.4 \pm 0.2$ |
| 1-6 | $1.6 \pm 0.9$ | $< 0.6$ | $2.4 \pm 0.2$ | $1.32 \pm 0.08$ | 0.9 | $> 3.7$ |
| 2-1 | $2.8 \pm 0.7$ | $0.2 \pm 0.1$ | $3.1 \pm 0.2$ | $1.43 \pm 0.06$ | 1.2 | $> 4$ |
| 2-2 | $14 \pm 1$ | $0.7 \pm 0.2$ | $8.2 \pm 0.5$ | $1.85 \pm 0.06$ | 1.5 | $3.9 \pm 0.2$ |
| 2-3 | $9.7 \pm 0.2$ | $1.4 \pm 0.5$ | $13 \pm 2$ | $2.0 \pm 0.1$ | 1.5 | $3.2 \pm 0.2$ |
| 2-4 | $3.5 \pm 0.5$ | $0.5 \pm 0.1$ | $6.5 \pm 0.9$ | $1.7 \pm 0.1$ | 1.3 | $3.2 \pm 0.2$ |
| 2-5 | $2.5 \pm 0.5$ | $< 0.5$ | $3.1 \pm 0.2$ | $1.43 \pm 0.06$ | 1.0 | $> 4$ |
| 2-6 | $1.3 \pm 0.6$ | $< 0.5$ | $2.8 \pm 0.3$ | $1.4 \pm 0.1$ | 0.8 | $> 3.2$ |

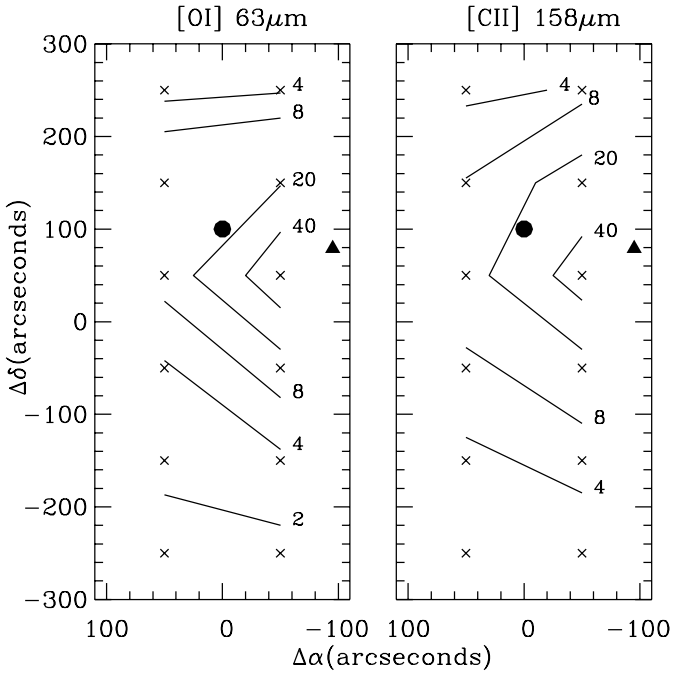


**Fig. 7.** Isophotal contours of [OI]63$\mu$m and [CII]158$\mu$m line emission in NGC 7129. Numerical values are expressed in $10^{-19}$ W cm$^{-2}$. The locations of the sources LkH$\alpha$234 and BD+65°1637 are identified with a full circle and triangle respectively. The position (0,0) refers to the ISO-LWS map center while the crosses indicate the centers of the 12 individual pointings: the position labelled (1-1) in Table 6 corresponds to the upper right corner while (2-6) to the lower left one.

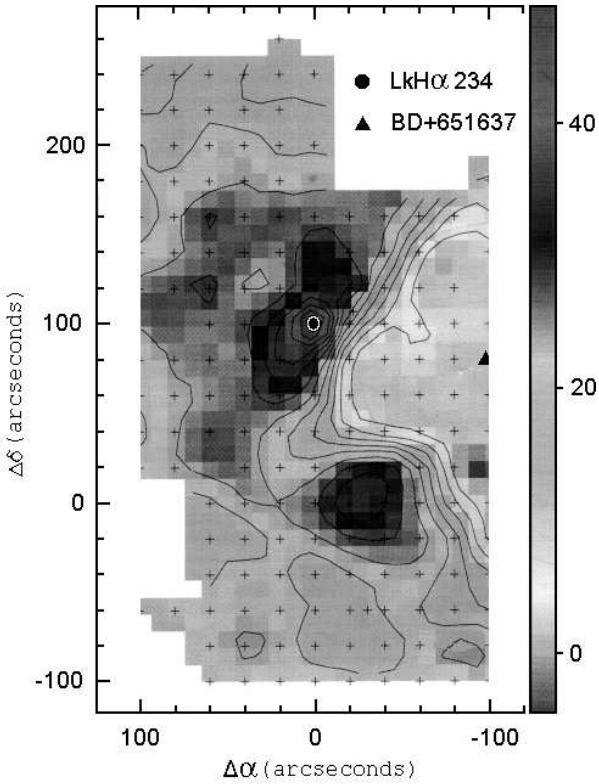


**Fig. 8.** Integrated intensity map of the $^{13}$CO line obtained by Fuente et al. (1998), adapted to reproduce both the same locations of the sources and the offset positions as in Fig. 7.

plot the locations of the two Herbig stars in the field, namely LkH$\alpha$234 and BD+65°1637, are also indicated. The ratio between the [OI] 63$\mu$m and [CII] 158$\mu$m line fluxes is always $<$ 2, as expected if photodissociation dominates (HTT); moreover the morphology of the line emission suggests that a low density PDR is more likely illuminated by the star BD+65°1637, whereas another more dense PDR is associated with LkH$\alpha$234 (see 5.1 and 5.5). This hypothesis is supported by the distribution of the molecular emission obtained, at a comparable scale, by Fuente et al. (1998). Their $^{13}$CO J=1-0 data, adapted in Fig. 8 to have the same offset as in Fig. 7, clearly shows both the cavity excavated by BD+65°1637, coincident with the peak of the FIR atomic line emission, and the ridge of the nearby molecular cloud in which LkH$\alpha$234 is partially embedded. To assess this possibility quantitatively, we have used the [CII] 158$\mu$m flux observed in each position to derive the value of the FUV radiation field $G_o$, using the relationship applicable to low density PDR's: $I_{CII} \sim 10^{-6} G_o$ ergs cm$^{-2}$ s$^{-1}$ sr$^{-1}$, where $G_o$ is measured in

units of 1.6 $10^{-3}$ ergs cm$^{-2}$ s$^{-1}$ (HTT). The derived values of $G_o$ are reported in Table 6 (Column 5) along with those expected for BD+65°1637 (Column 6), given its projected distance from the ISO beam center. We have adopted a luminosity of 2400 $L_\odot$ (Hillenbrand et al. 1992), and a FUV (between 6 and 13.6 eV) field which is 40% of the total luminosity of a B3 star. The error on these latter $G_o$ values is estimated by assuming uncertainties of 20% to both the flux and distance. There is a surprising agreement between the two evaluations of $G_o$, in fact the observed values (Column 5) systematically exceeds those due to the star (Column 6) by a constant and very low value $G_o$ = 2.5±0.5, which likely is due to a constant and diffuse component. This indicates the presence of a PDR illuminated by BD+65°1637 at the edge of the molecular material reported by Fuente et al. (1998). Using the derived value of $G_o$ and the intensity ratio [OI] 63$\mu$m/[CII] 158$\mu$m, we can *a posteriori* verify that our assumption of a low density PDR is correct, with the density in each individual position remaining below $10^4$ cm$^{-3}$; indeed, the derived values for log n (Column 7) range from 2.6 to 3.9, and are fully consistent with the density gradient reported by Fuente et al. (1998). Further evidence for a PDR associated with this region, has been recently provided by Schultz et al. (1997): they obtained NIR images of the edge structure in the filters $H_2$ 1-0 S(1) and 2-1 S(1), deriving for the ratio 1-0/2-1 S(1) a value expected for fluorescent rather than shocked $H_2$. They ascribe the PDR to originate in the material illuminated by the UV field from BD+65°1638, whereas we suggest the Herbig star BD+65°1637 because of both its location, which is more consistent with the edge morphology traced by $^{13}$CO emission, and the very good agreement found in the derived parameters ($G_o$ and density). Finally, we remark that high-J CO emission has been observed only towards the LkH$\alpha$234 position, and hence it cannot be related with the large scale, low density PDR we have so far considered. We will show in Sect. 5.5 (and fully discuss in Paper II) that these lines originate in the clumpy and denser PDR associated with LkH$\alpha$234 itself.

### *5.3. MWC 1080 line mapping*

In order to spectroscopically cover the sky area of an isotropic CO outflow emanating from MWC 1080, we have obtained four (2×2) adjacent pointings covering a square area centered about 20 arcsec to the south of MWC 1080. Given the proximity of the scan positions, the additional pointing *on* source partially overlaps all the four map elements. Because of such an overlap, it is not possible to do a proper *on-off* source subtraction, however such a subtraction has the marginal consequence of relocating this source in slightly different $(x, y)$ position in Fig. 4 (labelled as ON-OFF to distinguish it from the unsubtracted position, ON). The values reported in Tables 3 and 4 for the [OI] 63$\mu$m and [CII] 158$\mu$m line intensities, measured *on* source and on the four scans positions, respectively show a centrally peaked distribution which suggests the central object as the likely exciting source. Again, the [CII] intensity is more uniform when compared with the [OI] emission. By applying the same procedure adopted in the previous case (NGC 7129), we estimate the radiation field due to the star at the center of each map position ($i.e.$ ∼ 0.3 pc from MWC 1080): apart minor differences arising from the fact that MWC 1080 is not exactly on the center of the 4 pointings (but ∼ 20 *arcsec* to the North), we obtain a value of log$G_o$ = 3.5 using the luminosity and distance given in Table 1 and adopting as FUV field from a B0 star the 54% of its total luminosity. Contrasting with this are the observed [CII] line intensities, which are compatible with a value of log$G_o$ ∼ 1.8 (HTT). This apparent disagreement is reconciled by the observations by Fuente et al. (1998): MWC 1080 lies in a peak of molecular emission which obviously produces extinction effects on the stellar field created by the embedded object. They give an estimate of the mass within a radius of 0.08 pc from MWC 1080 which is 3.3 or 10.5 $M_\odot$ according to mm-continuum or line observations respectively. From these values the column density $N_H$ can be estimated to range between 1.9 $10^{22}$ and 6.3 $10^{22}$ cm$^{-2}$; through the relationship $N_H$ = 2.5 $10^{21}$ $A_V$ (usually adopted in dense clouds) we obtain 3.8 and 12.1 mag for $A_V$ to the observer, which can be converted in $A_{UV}$ (Cardelli et al. 1989) giving 5.7 and 18.1 mag respectively. Aiming to compare these values with our observations, we estimate the ratio between the expected radiation field at 0.08 pc, i.e. $G_o \sim 10^5$, with the value $G_o$ = 50-100 derived by the fine structure lines present in the *on* source position. The resulting extinction of a factor ∼ $10^3$ means $A_{UV}$ ∼ 7.5 mag which is within the range derived by Fuente et al.

In other words the stellar field is lower than expected (taking into account just geometrical dilution) not only in the *off* source position, but *on* source as well, since it suffers the major extinction in a compact region close to the star, whose size (r ≤ 0.08 pc) is lesser than the LWS beam. This is the reason why [CII] line emission has a comparable intensity everywhere, both *on* and *off* source.

Molecular line emission in form of CO rotational transitions (J=17-16, J=15-14) is clearly seen in the NW and SE positions of the map, and can be recognised at a lower S/N ratio also in the other beams. The observed lines are inadequate for deriving the physical parameters of the emitting region, nevertheless, if they likely represent the peak of the intensity distribution, they than suggest that the temperature of the molecular gas lies between 500 and 1000K (Paper II).

From Table 4 we have indication for the presence of a ionised region where the [OIII] 88$\mu$m emission originates. This line is not detected *on* source, probably because of the strong continuum: the 3$\sigma$ upper limit derived from the *rms* continuum fluctuations is comparable to the detected *off* source fluxes. This value is reported in Table 7 along with other ionic lines limits which will be useful in the following discussion. Here we note that the ratios [OIII] 88$\mu$m / [OIII]52$\mu$m calculated on the positions (1-2) and (2-2) are ∼ unity, indicating an ionised environment with a low electron density $\lesssim$100 cm$^{-3}$) (Rubin et al. 1994).

### *5.4. Ionised lines*

As expected, the intermediate ionisation fine structure emission lines are associated only with those HAEBE having spectral

types earlier than B0, namely CoD-42° 11721, V645 Cyg and MWC 1080. The latter has been discussed in Sect. 5.3, while the line fluxes detected both *on* and *off* source and the $3\sigma$ upper limits for CoD-42° 11721 and V645 Cyg are given in Tables 4, 5 and 8 respectively. Unfortunately the [OIII] $^3P_2 - ^3P_1$ transition at 52 $\mu$m falls in the SW2 detector which has one of the worst sensitivities (Swinyard et al. 1998), and the [NII] $^3P_1 - ^3P_0$ at 205 $\mu$m lies just beyond the cut-off wavelength of the LWS. Such unfavourable circumstances prevent us from deriving the relevant ionic pair intensity ratios [OIII] 52/88 and [NII] 122/205, nevertheless we can constrain both the electron density and the size of the ionised region.

In the case of CoD-42° 11721 the HI recombination lines and the consequent reconsideration on the distance to the source ($\sim$ 500 pc) are discussed in Benedettini et al. (1998). Here, the ionic lines which are relevant for the present discussion are reported in Table 3. To derive the parameters of the ionised region we follow the method illustrated by Rubin et al. (1994) without explicitly quoting their relationships and plots. The two $\Delta$J=1 FIR fine structure transitions for species with a $^3$P ground state are important indicators of the electron density ($N_e$), suffering a marginal dependence on the electron temperature with respect to the near IR/optical lines of the same species. Here we compare two estimates, namely $N_e$(OIII) and $N_e$(SIII) from the observed line ratios [OIII] 88/52 and [SIII] 33/19 respectively. The upper limit on the 52 $\mu$m line flux (Table 7) allows an upper limit to be placed on the $N_e$(OIII) $< 6\ 10^2$ cm$^{-3}$. The value of the ratio [SIII] 33/19 reported in Table 7 has been corrected both for the different beam size of the SWS at the two wavelengths (de Graauw et al. 1996) and for interstellar extinction, which marginally affects the 19$\mu$m line. Following Simpson et al. (1995), we adopted $\tau_{19\mu m} = 0.35 \cdot \tau_{9.7\mu m}$, where $\tau_{9.7\mu m}$ was derived as the ratio $A_V$/16.6 (Rieke & Lebofsky 1985). As a result we estimate $N_e$(SIII) = $4 \pm 3\ 10^2$ cm$^{-3}$. The agreement between the $N_e$ independent estimates suggests the presence of a low and constant density ionised volume, where $O^{++}$ and $S^{++}$ substantially overlap. Moreover, given the ionisation potentials of the two species (35.1 eV for $O^+$ and 23.3 ev for $S^+$), the fact that $N_e$(OIII) $\lesssim$ $N_e$(SIII), rules out a decreasing density gradient from the central exciting source.

A similar diagnostic cannot be applied for the *off* source positions (Table 7), where no SWS observations have been obtained. The derived upper limit for $N_e$(OIII) is obviously less compelling than those *on* source, because while [OIII] 88$\mu$m emission decreases increasing the distance from the star, [OIII] 52$\mu$m limit remains constant. The similar behaviour (*on* and *off* source) of the [NII] 122$\mu$m intensity (Tables 3 and 4) confirms that the central star is the major source of excitation. This finding and especially that about its proximity, are quite important since they question the association of CoD-42° 11721 (IRAS 16555-4237) with a bright rimmed cloud illuminated by the HII region RCW 113/116, which was suggested by Sugitani & Ogura (1994) who adopted a distance to the object of about 2 kpc.

Commonly in HII regions, the dominant ionisation states of the most abundant heavy elements S and N are $S^{++}$ and the $N^+$, $N^{++}$ respectively. Therefore in an optically thin region, the ratios $S^{++}/H^+ = (F_{19}/\epsilon_{19})/(F_H/\epsilon_H)$ and $(N^+ + N^{++})/H^+ = (F_{57}/\epsilon_{57} + F_{122}/\epsilon_{122})/(F_H/\epsilon_H)$ ($\epsilon = j_\lambda/(N_e N_i$, $j_\lambda$ is the volume emissivity for the line and $N_e$, $N_i$ the electron and ion densities) should provide a measure of the abundances of both species. By assuming the $\epsilon$ values given in Rubin et al. (1994), we find abundances much lower (by a factor $\sim 10^2$) than expected for both species. This occurence, i.e. that there is much more hydrogen than expected, can be explained in terms of different emitting regions having different opacities. According to the conclusion by Benedettini et al. (1998), based upon ISO-SWS HI recombination lines, a compact and optically thick HII region is expected around CoD-42° 11721 where the ionic fine structure lines remain undetected because of their critical densities. On the contrary these lines likely originate in a dilute and optically thin region, as suggested by the low electron density derived before. While in the same paper the radius of the compact HII region is estimated to be 3.6 $10^{12}$ cm, the size (R) of the fine structure line emission region can be obtained by the relationship:

$$L_{OIII(88\mu m)} = A \cdot n_{up} \cdot h\nu \cdot \frac{4}{3}\pi R^3 \qquad (1)$$

where $L_{OIII}$ is the line luminosity at the given distance, *A* is the Einstein coefficient of the fundamental transition $^3P_1 - ^3P_0$ at 88$\mu$m, $n_{up}$ is the thermal population of the $^3P_1$ level (at $10^4$K), and $\nu$ is the transition frequency. By using $n_H = 10^2$ cm$^{-3}$, $n_H/n_{OIII} \approx 10^4$, we derive *R* = 3 $10^{17}$ cm, which exceeds by orders of magnitude the size of the HII region. The value of *R*, when compared with the radius of the ISO-LWS beam (2.4 $10^{17}$cm at this wavelength) is consistent with the presence of [OIII] and [NII] line emission also in the adjacent *off* source beams. We can have a further check of the above picture by: *(i)* deriving the relative abundance ratio:

**Table 7.** Ionic lines intensities and $3\sigma$ upper limits

| Source | [OIII] 52$\mu$m | [OIII] 88$\mu$m | [OIII] 88 | $N_e$(OIII) |
|---|---|---|---|---|
| | Flux ($10^{-19}$ W cm$^{-2}$) | | [OIII] 52 | (cm$^{-3}$) |
| CoD-42° 11721 *on* [a] | $< 24$ | $15 \pm 3$ | $> 0.6$ | $< 6\ 10^2$ |
| CoD-42° 11721 *off* W | $< 30$ | $7 \pm 1$ | $> 0.2$ | – |
| CoD-42° 11721 *off* E | $< 19$ | $5 \pm 2$ | $> 0.2$ | – |
| V645 Cyg *on* | $< 5.7$ | $5.4 \pm 0.9$ | $> 0.9$ | $< 2\ 10^2$ |
| V645 Cyg *off* W | $< 6.1$ | $8.3 \pm 0.4$ | $> 1.4$ | – |
| V645 Cyg *off* E | $< 4.9$ | $8.7 \pm 0.3$ | $> 1.8$ | – |
| MWC 1080 *on* | $< 0.7$ | $< 1.3$ | – | – |
| MWC 1080 (1-2) | $< 1.8$ | $1.7 \pm 0.4$ | $> 0.9$ | $< 10^2$ |
| MWC 1080 (2-2) | $< 1.2$ | $1.4 \pm 0.4$ | $> 1.2$ | $< 10^2$ |

*Note to the Table:*

a [SIII] lines have been also observed, giving [SIII]33/[SIII]19 = $1.3 \pm 0.5\ 10^{-19}$ W cm$^{-2}$, then a value of $N_e$(SIII) = $4 \pm 3\ 10^2$ cm$^{-3}$ can be derived.

$$\frac{S}{N} = \frac{SIII}{NII + NIII} = \frac{F_{19}/\epsilon_{19}}{F_{57}/\epsilon_{57} + F_{122}/\epsilon_{122}} \quad (2)$$

which is unrelated to the hydrogen content and then by *(ii)* comparing it with the expected value for a thin region. The lack of detection of the 57$\mu$m line prevents its use in studying the abundance ratio, but one can easily check that ($F_{57}/\epsilon_{57}$) < 0.9 · ($F_{122}/\epsilon_{122}$); thus the resulting abundance ratio should be multiplied by a factor between 1 and 1.9. Considering beam size and extinction effects, we obtain from the observed [SIII] and [NII] lines the value S/N = 0.07 which agrees well with the value = 0.12 found by Rubin et al. (1991) in modeling Orion.

We note that an estimate of the effective temperature of the exciting object relies on the ratio [SIII] 19,33$\mu$m/ [OIII] 52$\mu$m, or, alternatively, on the fractional ionisation $<N^{++}>/<N^{+}>$ = ($F_{57}/\epsilon_{57}$)/($F_{122}/\epsilon_{122}$). The lack of a clean detection of both the 52$\mu$m and 57$\mu$m line is consistent with the spectral type B0 assigned to this star (Figs. 2 and 4 of Rubin et al. 1994).

Before our recent ISO-SWS observations (Benedettini et al. 1998) CoD-42° 1172 was spectroscopically observed in the UV (Shore et al. 1990), optical (Hutseméker & Van Drom 1990) and near IR (McGregor & Hyland 1988) spectral regions. A general consensus exists about spectral variability on long timescales and the presence of a dense shell with an ionised stellar wind is required to account for optically thick HI lines and the HeI emission. Contrasting with other evidence, Hutseméker & Van Drom (1990) provided a tentative interpretation in favour of the evolved nature of the star, since the optical spectrum shows signs of processed material (from the [NII] and [SII] lines along with a lack of detection of oxygen forbidden lines). Our FIR data do not allow a conclusive diagnostic in this sense, but, indicating the presence of ionised regions at different densities, suggests that density gradients, more than abundance gradients, are responsible for the observed line ratio.

In the case of V645 Cyg, only the [OIII] 88$\mu$m line has been detected both *on* and *off* source (Table 7), thus the diagnostic value is poor. Using the same method as before, we derive low values for the electron density $N_e \lesssim 2\ 10^2$ cm$^{-3}$ and a size for the emitting region *R* = 1.4 $10^{18}$ cm, which is smaller than the ISO beam (3.6 $10^8$ cm).

### *5.5. Molecular lines*

In Sect. 5.1 we have provided evidence for a high density environment around two sources of our sample (RCrA and IRAS12496-7650). Moreover Fuente et al. (1998) have shown that LkH$\alpha$234, MWC 1080 and LkH$\alpha$198 are located within a density peak. For all these sources, where increased column density is expected, we have also observed CO emission from rotational lines with quantum numbers in the range between J=14 to J=21 (see Table 3). The first three objects (RCrA, IRAS12496-7650 and LkH$\alpha$234), which also have substantial molecular emission are discussed in Paper II. In that paper, the likely excitation mechanism is suggested to be photodissociation in a clumpy medium rather than C-shock or J-shock processes, although high J CO emission is detected in our sample whenever a CO outflow does occur.

## 6. Conclusions

The main conclusions of this work can be summarised as follows:

- ISO-LWS allowed us to obtain the first detections of fine structure and molecular lines for a significant sample of HAEBE.
- [OI] 63$\mu$m and [CII] 158$\mu$m lines are observed in all the sources. The emission is often extended and [OI] is definitely more intense *on* source, while [CII] tends to have comparable intensities in nearby *off* source positions.
- The [OI] 145$\mu$m line has been detected toward four objects, while useful upper limits are derived for the remaining stars. The [OI], [CII] line ratios clearly indicate that the photodissociation mechanism can be considered as the main excitation source for these lines in HAEBE, rather than shock processes.
- Although there are a number of upper limits and relatively large errors, some diagnostic of the PDR (FUV field and density), according to the current models, is given. In a not negligible number of cases the ratio 63/145 is anomalously less than expected. A possible reason is that [OI] at 63$\mu$m could be self-absorbed by cold oxygen along the line of sight. This suggests some reconsideration of the PDR models which include a more realistic morphology of the emitting region.
- A clear case of PDR emission is presented for the region NGC 7129, for which we have obtained a spectroscopic map of the relevant part of the region.
- Intermediate ionisation fine structure lines [OIII], [NII] are associated with the HAEBE having spectral types earlier than B0. The case of CoD-42° 11721 is discussed in more detail due to the detection of complementary lines ([SIII]) in its SWS spectrum. An extended low electron density region is found, which lies external to a more compact and optically thick region where HI recombination lines originate.
- Although molecular line emission is associated with the stars having a CO outflow, FUV irradiaton in a clumpy medium accounts for the observed data much better than C-shock models. Therefore photodissociation (allowing some clumpiness) represents the main mechanism of both atomic and molecular gas excitation in HAEBE.

*Acknowledgements.* We would like to express our deep thanks to Mike Luhman for providing us with his model results on PDR line emission before the publication.

## References

Baluteau J.-P., Cox P., Cernicharo J., et al., 1997, A&A 322, L33
Bechis K.P., Harvey P.M., Campbell M.F., Hoffmann W.F., 1978, ApJ 226, 439
Benedettini M., Nisini B., Giannini T., et al., 1998, A&A 339, 159
Berrilli F., Corciulo G., Ingrosso G., et al., 1992, ApJ 398, 254
Brooke T.Y., Tokunaga A.T., Strom S.E., 1993, AJ 106, 656
Burton M.G., Hollenbach D.J., Tielens A.G.G., 1990, ApJ 365, 620
Cabrit S., Lagage P.O., McCaughrean M., Olofsson G., 1997, A&A 321, 523

Cantó J., Rodriguez L.F., Calvet N., Levreault R.M., 1984, ApJ 282, 631
Cardelli J.A., Clayton G.C., Mathis J.S., 1989, ApJ 345, 245
Clegg P.E., Ade P.A.R., Armand C., 1996, A&A 315, L38
Chokshi A., Tielens A.G.G.M., Werner M.W., Castelaz M.W., 1988, ApJ 334, 803
Cohen M., Hollenbach D.J., Haas M.R., Erickson E.F., 1988, ApJ 329, 863
de Graauw T., Haser N.L., Beintema D.A., 1996, A&A 315, L49
Diaz-Miller R.I., Franco J., Shore S.N., 1998 ApJ 501, 192
Di Francesco J., EvansII N.J., Harvey P.M., Mundy L.G., Butner H.M., 1994, ApJ 432, 710
Di Francesco J., EvansII N.J., Harvey P.M., Mundy L.G., Butner H.M., 1998, ApJ 509, 324
Draine B.T., Roberge W.G., Dalgarno A., 1983, ApJ 264, 485
Edwards S., Snell R.L., 1983, ApJ 270, 605
Ferderman S.R., Knauth D.C., Lambert D.L., Andersson B.-G., 1997, ApJ 489, 758
Fuente A., Martin-Pintado J., Chernicharo J., Bachiller R., 1990, A&A 237, 471
Fuente A., Martin-Pintado J., Cernicharo J., Brouillet N., Duvert G., 1992, A&A 260, 341
Fuente A., Martin-Pintado J., Bachiller R., Neri R., Palla F., 1998, A&A 334, 253
Giannini T., Lorenzetti D., Tommasi E., et al., 1999, A&A (this issue) (Paper II)
Habing H.J., 1968, Bull. Astr. Inst. Netherlands 19, 421
Harvey P.M., Lada C.J., 1980, ApJ 237, 61
Henning Th., Launhardt R., Steinacker J., Thamm E., 1994, A&A 291, 546
Henning Th., Burkert A., Launhardt R., Leinert Ch., Stecklim B., 1998, A&A 336, 565
Hillenbrand L.A., Strom S.E., Vrba F.J., Keene J., 1992, ApJ 397, 613
Hollenbach D., 1985, Icarus 61, 36
Hollenbach D., McKee C.F., 1989, ApJ 342, 306
Hollenbach D., Takahashi T., Tielens A.G.G.M., 1991, ApJ 377, 192 (HTT)
Hutseméker D., Van Drom E., 1990, A&A 238, 134
IRAS Science Team, 1986, A&AS 65, 607
Kaufman M.J., Wolfire M.G., Hollenbach D., Luhman M.L., 1998, ApJ submitted
Kessler M., Steinz J.A., Anderegg M.E., 1996, A&A 315, L27
Kraemer K.E., Jackson J.M., 1998, ApJ 503, 785
Lagage P.O., Olofsson G., Cabrit S., et al., 1993, ApJ 417, L79
Levreault R.M., 1988, ApJ 330, 897
Liseau R., White G., Larsson B., et al., 1998, A&A submitted
Malfait K., Waelkens C., Waters L.B.F.M., et al., 1998, A&A 332, L25
McGregor P.J., Hyland A.R., 1988, ApJ 324, 1071
Mitchell G.F., Matthews H.E., 1994, ApJ 423, L55
Natta A., Palla F., Butner H.M., EvansII N.J., Harvey P.M., 1993, ApJ 406, 674
Nisini B., Milillo A., Saraceno P., Vitali F., 1995, A&A 302, 169
Nisini B., Lorenzetti D., Cohen M., et al., 1996, A&A 315, L321
Pezzuto S., Strafella F., Lorenzetti D., 1997, ApJ 485, 290
Prusti T., Natta A., Palla F., 1994, A&A 292, 593
Ray T.P., Poetzel R., Solf J., Mundt R., 1990, ApJ 357, L45
Rieke G.H., Lebofsky M.J., 1985, ApJ 288, 618
Rubin R.H., Simpson J.P., Haas M.R., Erickson E.F., 1991 ApJ 374, 564
Rubin R.H., Simpson J.P., Lord S.D., et al., 1994, ApJ 420, 772
Sandell G., Olofsson H., 1981, A&A 99, 80
Sandell G., Weintraub D.A., 1994, A&A 292, L1
Saraceno P., Nisini B., Benedettini M., et al., 1998, In: Yun J.L., Liseau R. (eds.) Proc. of Star Formation with the Infrared Space Observatory. ASP Conf.Series vol.132, p. 233
Schultz A.S.B., Rank D.M., Temi P., Holbrook J.C., 1997, In: Malbet F., Castets A. (eds.) Proc. of IAU Symp. No.182 Herbig-Haro Flows and the Birth of Low Mass Stars. p. 39
Simpson,J.P., Colgan S.W.J., Rubin R.H., Erickson E.F., Haas M.R., 1995, ApJ 444, 721
Shore S.N., Brown D.N., Bopp B.W., et al., 1990, APJS 73, 461
Sugitani K., Ogura K., 1994, APJS 92, 163
Swinyard B.M., Clegg P.E., Ade P.A.R., et al., 1996, A&A 315, L43
Swinyard B.M., Burgdorf M.J., Clegg P.E., et al., 1998, In: Flower A.M, (ed.) Infrared Astronomical Instrumentation SPIE 3354, p. 888
Tommasi E., Pezzuto S., Giannini T., et al., 1999, A&A submitted (Paper III)
Volk K., Cohen M., 1989, AJ 98, 931
Waelkens C., Waters L.B.F.M., de Graauw M.S., et al., 1996, A&A 315, L245
Weintraub D.A., Kastner J.H., Mahesh A., 1994, ApJ 420, L87
Wesselius P.R., van den Ancker M.E., Young E.T., et al., 1996 A&A 315, L197